Two-Dimensional Violet Phosphorus: A p-Type Semiconductor for (Opto)electronics

Antonio Gaetano Ricciardulli, Ye Wang, Sheng Yang, Paolo Samorì

Two-dimensional violet phosphorus: a p-type semiconductor for (opto)electronics

Antonio Gaetano Ricciardulli,[†] Ye Wang,[†] Sheng Yang,[‡] Paolo Samorì*,[†]

[†]University of Strasbourg, CNRS, ISIS UMR 7006, 8 allée Gaspard Monge, 67000 Strasbourg, France

[‡]Center for Advancing Electronics Dresden (cfaed) and Department of Chemistry and Food Chemistry, Technische Universität Dresden, Mommsenstrasse 4, Dresden 01069, Germany

ABSTRACT: The synthesis of novel two-dimensional (2D) materials displaying unprecedented composition and structure via the exfoliation of layered systems provides access to uncharted properties. For application in optoelectronics, the vast majority of exfoliated 2D semiconductors possess *n*-type or more seldom ambipolar characteristics. The shortage of *p*-type 2D semiconductors enormously hinders the extensive engineering of 2D devices for complementary metal oxide semiconductors (CMOS) and beyond CMOS applications. However, despite the recent progress in the development of 2D materials endowed with *p*-type behaviors by direct synthesis or *p*-doping strategies, finding new structures is still of primary importance. Here, we report the sonication-assisted liquid-phase exfoliation of violet phosphorus (VP) crystals into few-layer thick flakes and the first exploration of their electrical and optical properties. Field-effect transistors (FETs) based on exfoliated VP thin-films exhibit *p*-type transport feature with an I_{on}/I_{off} ratio of 10^4 and a hole mobility of 2.25 cm^2 V^{-1} s^{-1} at room temperature. In addition, the VP film-based photodetectors display a photoresponsivity (R) of 10 mA W^{-1} and a response time down to 0.16 s. Finally, VP embedded into CMOS inverter arrays display a voltage gain of ~17. This scalable production method and high quality of the exfoliated material combined with the excellent optoelectronic performances make VP an enticing and versatile *p*-type candidate for next-generation More-than-Moore (opto)electronics.

Introduction

The blooming of two-dimensional (2D) materials with complementary features and broadest variety of functionalities enabled tremendous progress in a broad range of applications, including electronics, optoelectronics, spintronics and beyond.[1–3] Novel paradigms in both fundamental and applied research have been disclosed by the assembling of *p-n* junctions based on 2D materials.[4–7] Nevertheless, their degree of freedom is limited by the scarcity in intrinsic *p*-type atomically thin structures, lagging behind the 2D materials exhibiting n-type behavior. So far, only a few species have been successfully identified, such as α-MnS, GaSe, InSe, WSe2, GeSe, GeS, 2D tellurium and selenium.[8–10] Despite their preliminary promising evidence, the device performances are hampered either by low carrier mobilities (i.e. ~ 10^{-1} cm^2 V^{-1} s^{-1} for 2D selenium and α-MnS) or harmful chemicals used for the synthetic process. In the quest of finding viable alternatives, *p*-type conduction in 2D materials has been mainly carried out by electrical gating, contact engineering and chemical/electrostatic doping of *n*-type or ambipolar 2D materials.[11,12] Although *p*-doping strategies have witnessed a rapid ascent in the recent years, they generally require additional cumbersome, expensive and high energy-input fabrication processes hindering their potential incorporation for large-scale applications. For example, chemical doping of 2D semiconductors, which is an effective route to tune the conduction type of the materials,

cannot be easily standardized and it suffers from the destructive impact on the structure and reduced long-term stability.[13,14] Therefore, novel *p*-type 2D materials are highly sought after as they would allow to enrich the current limited portfolio and would be instrumental for the development of both complementary *n-p* architectures and pristine *p*-electronic devices that have not been explored up to date.

As time progresses, more and more atomically thin materials are prepared. Among them, the elements from the group V, where phosphorus is the most representative, have recently drawn much attention for their interesting electrical, phonon and optical characteristics at the atomic limit.[15,16] For instance, black phosphorus (BP) features thickness-dependent direct bandgap,[17] unusual in-plane anisotropy,[18] high carrier mobilities[19] and large absorption coefficients.[20] Further, BP is an ambipolar semiconductor that undergoes *p*-doping by either interfacial charge transfer or covalent functionalization, which opens up novel possibilities in emerging dynamic (opto)electronic devices based on ambipolar semiconductors.[21,22] However, surface encapsulation is generally required to protect BP sheets from ambient degradation. Alternatively, violet phosphorus (VP), as being a more stable phosphorus allotrope,[23] has been theoretically predicted to exhibit hole mobilities of up to 7000 cm^2 V^{-1} s^{-1} and moderate-direct bandgap of 2.5 eV in its monolayers, making them ideal candidates
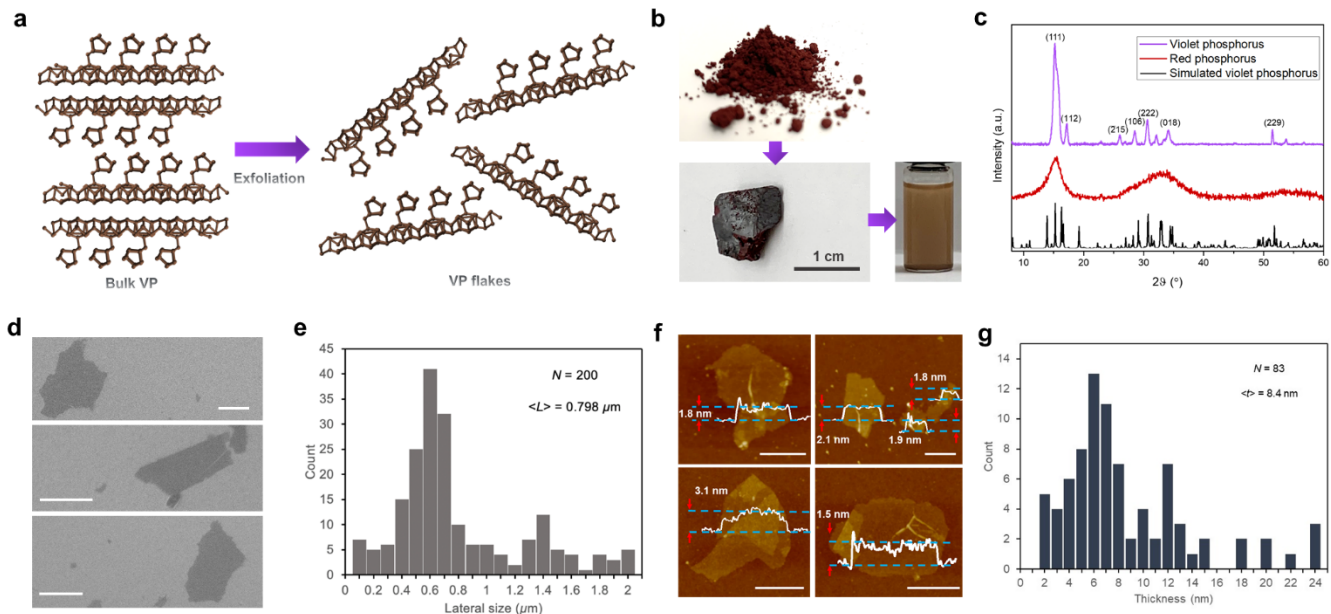
Figure 1. Synthesis and delamination of bulk VP. (a) Illustration of the exfoliation of VP. (b) The road to exfoliated VP. Optical images of amorphous red phosphorus used as precursor (top), as-synthesized VP crystal (bottom left) and stable dispersion of exfoliated VP flakes in DMF (bottom right). (c) XRD of smashed VP crystal, amorphous red phosphorus used as reagent and simulated pattern from the CIF[29] of VP. (d) Representative SEM images of liquid-phase exfoliated VP sheets. The scale bar is 1 μm. (e) Histogram of the lateral size distribution obtained from the analysis of 200 individual VP flakes. (f) AFM topographical images of spin-coated VP sheets onto SiO₂ substrate. The scale bar is 500 nm. (g) Histogram from the height profile of the AFM images of 83 randomly selected VP flakes.

for optoelectronic applications in the blue-color regime.[24] Nonetheless, the experimental access to such fascinating properties is still challenging. For instance, VP crystals with reduced sizes prefers to grow along with BP, making the separation and the purification of VP difficult.[23] Due to the brittle P-P bonds and interlayer interaction between P8 cages, the exfoliation of VP crystal inevitably leads to thick and small fragments.[23] So far, only few attempts on the exfoliation of bulk VP have been performed. However, most VP flakes exhibit high thicknesses (up to ~100 nm) and reduced lateral sizes, which severely limited their property exploration.[25] Therefore, it is critical to design a reliable synthetic strategy for preparing high-quality 2D VP sheets. In particular, the crystal growth and exfoliation process must be well studied to overcome the drawbacks arising from the current methods.

In this work, the electrical properties of high-quality liquid exfoliated VP flakes have been explored. First, the crystal growth of centimeter (cm) scale VP was achieved by controlling the nucleation process to avoid the formation of BP as by-product. Then, a series of solvents were carefully selected to peel off the thin sheets from the parent crystals under mild sonication. The exfoliated sheets exhibit large lateral dimensional size (up to 2 μm) and thicknesses down to the monolayer limit, with mean value as low as 8.4 nm. As a result, such scalable, solution-processed method enables various VP-based thin-film electronics. Field-effect transistors (FETs) exhibit distinct *p*-type transport characteristics with hole mobilities up to 2.25 cm² V⁻¹ s⁻¹ and high I_{on}/I_{off} ratio of 10^4 at room temperature, exceeding most of the reported thin-film 2D materials. Photodetectors show photoresponsivity of 10 mA W⁻¹ and a fast response time of 0.16 s in the UV region. Finally, we integrated VP as PMOS working material in a CMOS logic circuit. The NOR logic gate based on MoS₂ and VP nanosheets exhibit typical inverter characteristics with gain values as high as ~17,

which is comparable to record values in HfO₂ gated CMOS using 2D materials.[26] Our results indicate that VP holds enormous potential for the future development of fundamental and applied research in electronics and optoelectronics.

Results and Discussion

VP is a van der Waals layered material that can be exfoliated into thin flakes (**Figure 1a**). VP was synthesized via chemical vapor transport starting from amorphous red phosphorus as phosphorus source and tin and tin (IV) iodide as transport agents. In brief, the reagents were first intimately mixed and placed into a quartz tube, which was subsequently evacuated and sealed. Then, the mixture underwent to a controlled heating-cooling process (**Figure S1**, Supporting Information) to yield a large VP crystal with a lateral size of ~ 1 cm (**Figure 1b**). As BP can be easily formed as side product during the reaction,[27] it is critical to control the nucleation temperature and time. Generally, VP is embedded within the BP framework since the nucleation of BP, occurring at lower temperatures, proceed from VP during the cooling step.[28] Therefore, to preserve the integrity of VP, the nucleation temperature was set higher than that of the decomposition of BP (550 °C and 460 °C, respectively). Moreover, since the growth of VP is favored over BP on long nucleation time scales, the target
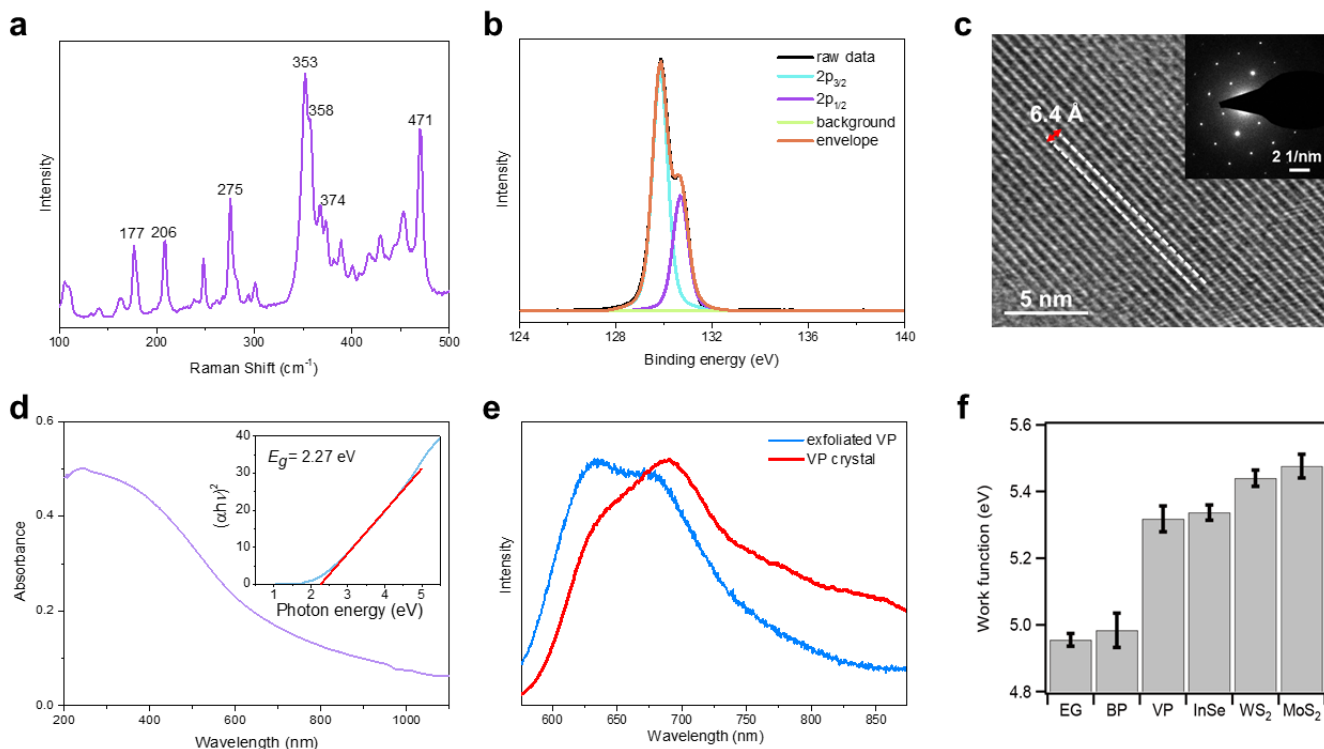
Figure 2. Structural, optical and electronic features of exfoliated VP. (a) Raman spectrum of VP film, excited by 532 nm laser. (b) High-resolution XPS spectrum of P 2p spectrum of a VP film. (c) Representative HR-TEM image of a VP flake. The inset shows the selected-area electron diffraction (SAED) pattern. (d) UV-vis-NIR absorption spectrum of exfoliated VP film on quartz. The inset shows the related Tauc plot. (e) Normalized PL of exfoliated VP versus bulk crystal. (f) Work function survey of different solution-processed films based on 2D materials obtained by PYSA and the related error bars (where EG is exfoliated graphene, InSe is indium selenide, WS_2 is tungsten disulfide and MoS_2 is molybdenum disulfide).

temperature was prolonged. To confirm the quality of the synthesized crystal, the product was investigated by X-ray diffraction (XRD; **Figure 1c**). The XRD measurement matches previous reports, indicating the distinct monoclinic $P2/c$ lattice structure of VP.[29]

To produce large quantities of VP sheets, sonication assisted liquid-phase exfoliation for 5 hours at 285 W was carried out. Among the different set of solvents used, *N,N*-dimethylformamide (DMF) yielded the most stable dispersion (**Figure S2**), hence it was chosen as a standard for further investigations. Scanning electron microscopy (SEM) analysis (**Figure 1d**) of VP flakes reveals a broad size distribution, with lateral dimensions up to 2 μm. Although the prolonged sonication induced the side fragmentation of larger flakes determining the presence of moderate amount of small VP fragments, the statistical analysis (**Figure 1e**) reveals that the majority of nanosheets display a lateral size in the range of 600-700 nm, being larger than previously reported liquid-phase exfoliated layered phosphorus analogues.[30,31] The statistical analysis on the thickness of the exfoliated VP performed from topographical profiles in atomic force microscopy (AFM; **Figure 1f**) images exhibited tight distribution with a mean value of 8.4 ± 5.0 nm (**Figure 1g, Figure S3**). In contrast, previously reported AFM heights of VP flakes are in the range of 30-100 nm.[25] These morphological results bear witness for the effectiveness of our liquid-phase strategy to delaminate bulk VP in a controlled fashion.

The structural features of the exfoliated VP were ascertained through Raman spectroscopy, transmission electron microscopy (TEM) and X-ray photoelectron spectroscopy (XPS)

analyses. The Raman spectrum of randomly selected area from a drop-cast film of VP flakes shows the characteristic modes of the material (**Figure 2a**).[32,33] The signals with strong intensity at the upper frequency range, 353, 358, 373 and 471 cm^{-1}, originate from the breathing and stretching modes of the phosphorus cages along the backbone (**Figure S4**). In contrast, the bands at the lower frequency range (< 290 cm^{-1}) result from the bond distortions and the rotational vibration of atoms. Such complexity of the Raman spectrum is due to the high number of atoms, 84, in the VP single unit cell. High-resolution XPS reveals that the band corresponding to P 2p appears at about 130 eV (**Figure 2b**), which can be divided into P $2p_{1/2}$ (130.66 eV) and P $2p_{3/2}$ (129.81 eV). It is noteworthy that the oxidized phosphorus feature, generally occurring at 134-136 eV for phosphorus architectures,[34,35] is absent, indicating the structural integrity of the synthesized VP sheets. To prevent the oxidation of the phosphorus structure, both synthetic and exfoliation processes were thoughtfully controlled. High-resolution TEM (HR-TEM) on a selected flake (**Figure S5**) displays a set of crystal planes with a lattice spacing of 6.4 Å (**Figure 2c**), which corresponds to the typical (110) lattice plane of monoclinic VP.[23] To reveal the optical characteristics of VP, ultraviolet–visible-near infrared (UV-vis-NIR) and photoluminescence (PL) spectroscopy on exfoliated VP was carried out. As shown in **Figure 2d**, the large absorption band of the drop-cast VP films (**Figure S6**) features a peak below 350 nm. The optical bandgap energy (E_g) was deduced to be 2.27 eV for exfoliated VP by the Tauc plot, which is higher than the value (1.7 eV) of the bulk counterpart.[23] As shown in **Figure 2e**, PL of VP is found to shift towards lower wavelengths upon exfoliation in accordance with the increasing

bandgap. Moreover, the broad PL response of the crystal at wavelengths above 740 nm is suppressed in the exfoliated sample, suggesting thickness-dependence in excitonic behaviors.[36]

To unveil the electrical performances of VP, drop-cast films were prepared. First, the work function (WF) of bare VP films was evaluated by photoelectron yield spectroscopy in air (PYSA). As shown in **Figure 2f**, VP exhibits a mean WF of 5.32 ± 0.03 eV, which is similar to the one measured for indium selenide (InSe) but ~0.3 eV higher than the other phosphorus allotrope BP. Hence, we speculate on the possible application of VP films as high-WF hole-injecting electrode materials in optoelectronics, including solar cells and light-emitting diodes, where high ionization potential semiconductors are commonly used as active materials.[37] We next fabricated bottom-contact, top-gated FETs based on VP films (**Figure 3a**). First, VP dispersion was drop-casted onto patterned interdigitated electrode devices on Si/SiO$_2$ substrates, where the SiO$_2$ thickness is 90 nm. Then, ion gel composed of a triblock copolymer, poly(styrene-block-ethylene oxide-block-styrene) (PS-PEO-PS) (7 wt%) blended with ionic liquid 1-ethyl-3-methylimidazolium-bis(trifluoromethylsulfonyl)imide ([EMIM][TFSI]), was readily coated on top of VP as top gate material. The transfer characteristics were recorded by sweeping a top gate voltage (V_g) and applying different bias voltages (V_{ds}) at room temperature (**Figure 3b** and **Figure S7**). Notably, a characteristic p-type behavior with an I_{on}/I_{off} ratio of 10^4 was obtained. The devices exhibit an average threshold voltage of -3.21 ± 0.25 V. Charge carrier mobility of VP film FETs was calculated by the following equation[38]:

$$\mu = \frac{L_{ch}}{W_{ch}C_{ox}V_{ds}}\frac{dI_{ds}}{dV_g}$$

$$(1)$$

where L and W are the channel length and width, respectively, and dI_{ds}/dV_g is the maximum slope extracted from the linear region of the transfer curves. Remarkably, our devices exhibited a mean hole mobility of 0.82 ($\pm$ 0.58) cm^2 V^{-1} s^{-1} determined over 13 devices (**Figure S8**) with the highest recorded value being 2.25 cm^2 V^{-1} s^{-1} (**Figure S9**), which is considerably higher than previously-reported FETs based on solution-processed 2D semiconductors films (**Table S1**).[39–41] High electric performances within the film result from the interplay of efficient intraflake and interflake transport. On the one hand, the intraflake transport is manifested in the high intrinsic mobility of VP which is determined by its unique electronic structure. Similarly to BP, large intrinsic hole mobility in VP occurs along one of the two directions (x and y) of the basal plane as a consequence of the strong anisotropy of the deformation potential in y (E_{1y}), which is extraordinarily smaller (0.18 eV) than the one along x.[24] On the other hand, the interflake transport is determined by the nature of the interflake contacts forming a network of nanosheets. High mobility is ascribed to the narrow thickness

distribution of thin VP flakes (**Figure 1g**), which enables the formation of a basal plane-aligned network of the exfoliated flakes along with reduced inter-sheet distance (**Figure S9**). This achievement leads to the creation of large-area and conformal inter-sheet junctions, which are responsible for the enhanced charge transport within the network.[42] Further, compared to single-flake FETs, charge transport in films based on solution-processed 2D materials is still limited by inter-flake resistances and structural defects induced by the exfoliation method. Nevertheless, the mobility arising from our thin film devices is still higher than the reported intrinsic mobilities of devices based on p-type single flakes like α-MnS and GaSe, 0.1 and 0.6 cm^2 V^{-1} s^{-1}, respectively.[8,43] Temperature-dependent resistance measurements in the range of 240 K and 330 K (**Figure 3c**) revealed that VP nanosheets exhibit semiconducting behavior. Furthermore, the charge injection activation energy (E_a) could be obtained by fitting the Arrhenius slopes of the ln(I_d) versus 1000/T curve.[44] We found (**Figure 3d**) an E_a of 409.624 meV, being on the same order of magnitude of liquid-phase exfoliated molybdenum disulfide (MoS$_2$).[41]
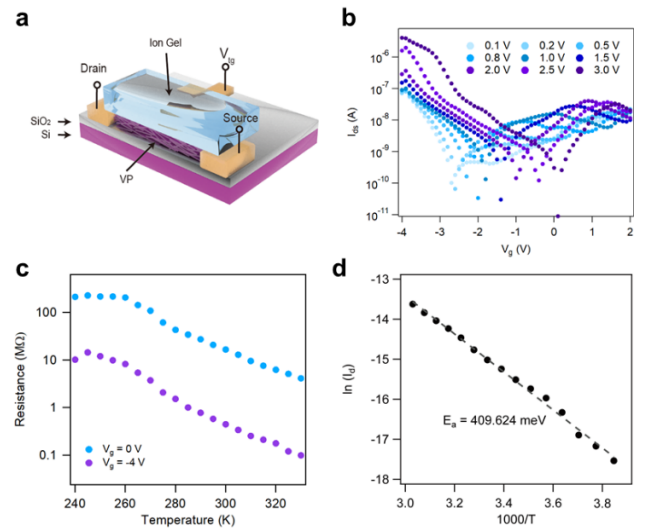

Figure 3. Electrical properties of VP films. (a) Schematic illustration of the FET based on drop-cast VP films. (b) Example of transfer characteristics of FET fabricated from VP at different voltages. (c) Temperature-dependent resistance of VP-based FET at different V_g values (0 V and -4 V, respectively) and (d) the corresponding Arrhenius plot at $V_g = 0$ V. The dashed line shows the fitting line of the Arrhenius slope for E_a calculation.

Recent reports revealed superior ambient stability of VP compared to BP.[45] Therefore, to assess the device stability, an FET based on VP film was stored in ambient conditions and the electrical performance tracked over a period of 12 days (**Figure S11**). Remarkably, the VP-based FET device exhibits high operational stability and slow performance degradation taking place only after 10 days, suggesting a good ambient stability of VP flakes which is also confirmed by AFM surface analysis (**Figure S12**).
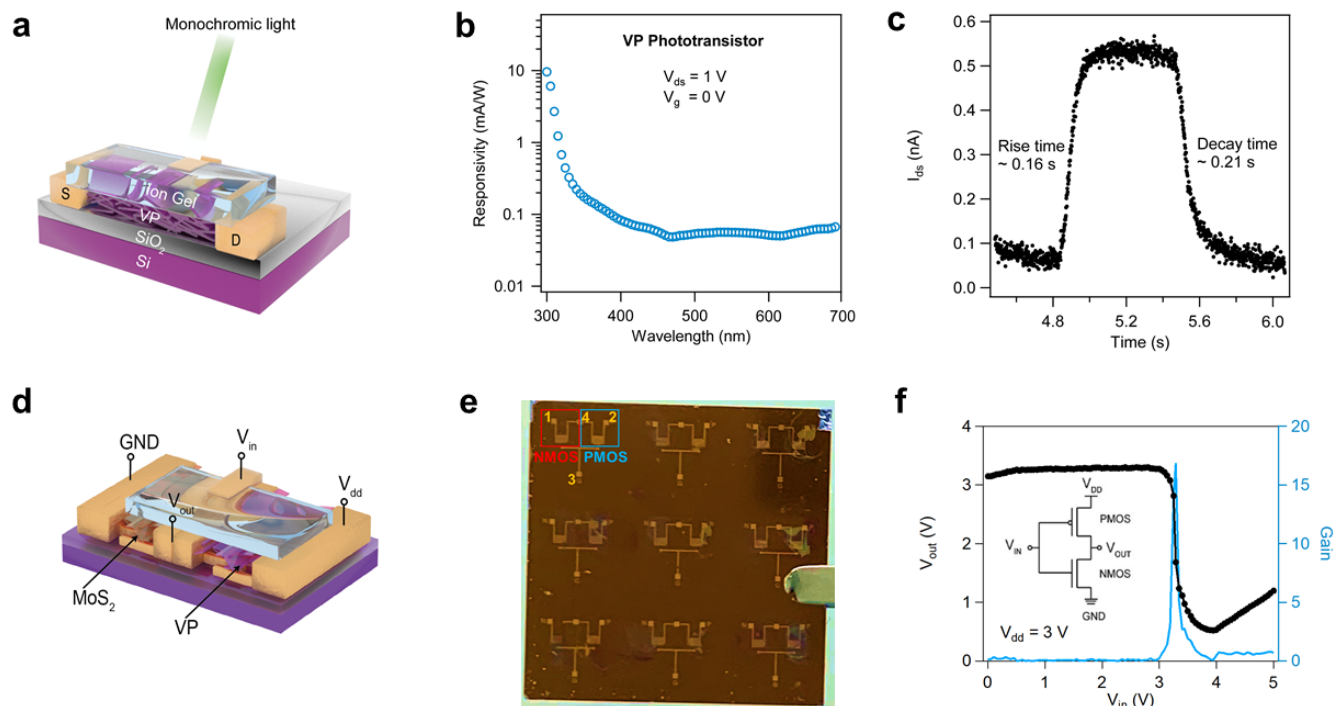
Figure 4. Proof-of-concept devices based on VP networks. (a) Schematic illustration of the phototransistor based on a drop-cast VP film. (b) Spectral responsivity of wavelength scan from 300 to 690 nm at V_{ds} = 1V and V_g = 0V. (c) Time-resolved photoresponse of the VP film at V_g = 0V and V_{ds} = 1V under the illumination of 365 nm. (d) Schematic representation of the CMOS inverter. (e) Optical image of the CMOS array. 1 is the ground (GND), 2 is the V_{DD}, 3 is the input voltage (V_{in}) and 4 is the output voltage (V_{out}). Channel length is 20 μm (f) V_{in}-V_{out} characteristics (black) and voltage gain (blue) of the MoS$_2$-VP logic inverter. The inset shows a schematic illustration of the electrical circuit.

In view of high conductance and strong PL intensity shown in VP films, we are interested in exploring the light-matter interactions of this new material. Optoelectronic characterizations were revealed by manipulating the VP FETs in phototransistor mode.

In order to rule out the influences of ion migration when light is illuminated on VP, we operate the photodetector at V_g = 0 V. The schematic architecture of the device configuration is illustrated in **Figure 4a**. The spectral photoresponse of incident light from 300 to 690 nm for VP (**Figure 4b**) reveals that the highest responsivity, 10 mA W^{-1}, over an area of 1 mm^2 occurs at 300 nm. As expected, the wide bandgap enables VP with maximum photoresponse in the UV region.[22] Moreover, stable photocurrent characteristics under illumination cycles at different wavelengths (**Figure S13**) suggest low trap density and long-term stability for VP-based phototransistors. As shown in **Figure 4c**, the rise and decay time for the device when switching on and off the laser light at 365 nm is 0.16 s and 0.21 s, respectively. It worth noting that our phototransistors operate at ultra-low voltages (V_g= 0 V and V_{ds}= 1 V), being compatible with low power consumption applications. Finally, we demonstrate a proof-of-concept CMOS circuit element containing VP nanosheets as one of the channel components, responding to the calls for new *p*-type semiconductors that would enable the realization of 2D-CMOS logic circuits. In our inverter, drop-casted VP and MoS$_2$ flakes were used for the *p*-type and *n*-type transistors (**Figure S14**, transfer characteristics of individual MoS$_2$-based FET), respectively. The architecture and optical image of the device are displayed in **Figure 4d** and **4e**, respectively. The inverter shows distinct binary output logic states of "1"and "0" by varying the input voltage from 0 V to 5 V (**Figure 4f**).

The sharp transition indicated a high voltage gain value of ~17, which is comparable to record values with HfO$_2$ gated CMOS based on liquid-phase exfoliated 2D materials.[26] The high logic manipulation efficiency envisions low power consumption computing in the next-generation CMOS technologies.

Conclusion

In conclusion, efficient exfoliation of bulk VP was achieved using a scalable solution-processable approach. The fabricated FETs based on VP films demonstrated a characteristic *p*-type conduction, responding to the urgent demand for novel *p*-type 2D semiconductors. Our samples exhibit mobilities up to 2.25 cm^2 V^{-1} s^{-1} and I$_{on}$/I$_{off}$ ratio of 10^4 at room temperature. Moreover, highest stable photoresponse is observed upon illumination at the UV range. As proof-of-concept, CMOS inverter from solution-processed VP as PMOS component has been demonstrated. Remarkably, high gain values have been achieved in our device. These findings make VP a promising candidate for future energy efficient large-area (opto)electronic applications. We believe that the combination of further fundamental studies together with the feasible device fabrication approach presented in our work, will provide a fertile playground for unveiling novel paradigms in the enticing landscape of *p*-type 2D semiconductors and beyond.

ASSOCIATED CONTENT

AUTHOR INFORMATION

Corresponding Author

*samori@unistra.fr

Author Contributions

All authors have given approval to the final version of the manuscript.

Notes

The authors declare no competing financial interests.

ACKNOWLEDGMENT

REFERENCES

(1)   Chen, H.; Xue, X.; Liu, C.; Fang, J.; Wang, Z.; Wang, J.; Zhang, D. W.; Hu, W.; Zhou, P. Logic Gates Based on Neuristors Made from Two-Dimensional Materials. *Nat. Electron.* **2021**, *4*, 399–404.

(2)   Kim, H.; Uddin, S. Z.; Lien, D.-H.; Yeh, M.; Azar, N. S.; Balendhran, S.; Kim, T.; Gupta, N.; Rho, Y.; Grigoropoulos, C. P.; Crozier, K. B.; Javey, A. Actively Variable-Spectrum Optoelectronics with Black Phosphorus. *Nature* **2021**, *596*, 232–237.

(3)   Ricciardulli, A. G.; Yang, S.; Smet, J. H.; Saliba, M. Emerging Perovskite Monolayers. *Nat. Mater.* **2021**, *20*, 1325.

(4)   Lee, C.-H.; Lee, G.-H.; van der Zande, A. M.; Chen, W.; Li, Y.; Han, M.; Cui, X.; Arefe, G.; Nuckolls, C.; Heinz, T. F.; Guo, J.; Hone, J.; Kim, P. Atomically Thin p–n Junctions with van Der Waals Heterointerfaces. *Nat. Nanotechnol.* **2014**, *9*, 676–681.

(5)   Chen, J.-W.; Lo, S.-T.; Ho, S.-C.; Wong, S.-S.; Vu, T.-H.-Y.; Zhang, X.-Q.; Liu, Y.-D.; Chiou, Y.-Y.; Chen, Y.-X.; Yang, J.-C.; Chen, Y.-C.; Chu, Y.-H.; Lee, Y.-H.; Chung, C.-J.; Chen, T.-M.; Chen, C.-H.; Wu, C.-L. A Gate-Free Monolayer WSe2 Pn Diode. *Nat. Commun.* **2018**, *9*, 3143.

(6)   Nassiri Nazif, K.; Kumar, A.; Hong, J.; Lee, N.; Islam, R.; McClellan, C. J.; Karni, O.; van de Groep, J.; Heinz, T. F.; Pop, E.; Brongersma, M. L.; Saraswat, K. C. High-Performance p–n Junction Transition Metal Dichalcogenide Photovoltaic Cells Enabled by MoOx Doping and Passivation. *Nano Lett.* **2021**, *21*, 3443–3450.

(7)   Rivera, P.; Yu, H.; Seyler, K. L.; Wilson, N. P.; Yao, W.; Xu, X. Interlayer Valley Excitons in Heterobilayers of Transition Metal Dichalcogenides. *Nat. Nanotechnol.* **2018**, *13*, 1004–1015.

(8)   Li, N.; Zhang, Y.; Cheng, R.; Wang, J.; Li, J.; Wang, Z.; Sendeku, M. G.; Huang, W.; Yao, Y.; Wen, Y.; He, J. Synthesis and Optoelectronic Applications of a Stable P-Type 2D Material: α-MnS. *ACS Nano* **2019**, *13*, 12662–12670.

(9)   Wang, Y.; Qiu, G.; Wang, R.; Huang, S.; Wang, Q.; Liu, Y.; Du, Y.; Goddard, W. A.; Kim, M. J.; Xu, X.; Ye, P. D.; Wu, W. Field-Effect Transistors Made from Solution-Grown Two-Dimensional Tellurene. *Nat. Electron.* **2018**, *1*, 228–236.

(10)   Qin, J.; Qiu, G.; Jian, J.; Zhou, H.; Yang, L.; Charnas, A.; Zemlyanov, D. Y.; Xu, C.-Y.; Xu, X.; Wu, W.; Wang, H.; Ye, P. D. Controlled Growth of a Large-Size 2D Selenium Nanosheet and Its Electronic and Optoelectronic Applications. *ACS Nano* **2017**, *11*, 10222–10229.

(11)   Peng, Q.; Si, C..; Zhou, J.; Sun, Z. Modulating the Schottky Barriers in MoS2/MXenes Heterostructrures via Surface Functionalization and Electric Field. *Appl. Surf. Sci.* **2019**, *480*, 199–204.

(12)   He, Q.; Liu, Y.; Tan, C.; Zhai, W.; Nam, G.; Zhang, H. Quest for P-Type Two-Dimensional Semiconductors. *ACS Nano* **2019**, *13*, 12294–12300.

(13)   Liu, X.; Qu, D.; Ryu, J.; Ahmed, F.; Yang, Z.; Lee, D.; Yoo, W. J. P-Type Polar Transition of Chemically Doped Multilayer MoS2 Transistor. *Adv. Mater.* **2016**, *28*, 2345–2351.

(14)   Nipane, A.; Karmakar, D.; Kaushik, N.; Karande, S.; Lodha, S. Few-Layer MoS2 p-Type Devices Enabled by Selective Doping Using Low Energy Phosphorus Implantation. *ACS Nano* **2016**, *10*, 2128–2137.

(15)   Mannix, A. J.; Kiraly, B.; Hersam, M. C.; Guisinger, N. P. Synthesis and Chemistry of Elemental 2D Materials. *Nat. Rev. Chem.* **2017**, *1*, 0014.

(16)   Miao, N..; Xu, B.; Bristowe, N. C.; Zhou, J.; Sun, Z. Tunable Magnetism and Extraordinary Sunlight Absorbance in Indium Triphosphide Monolayer. *J. Am. Chem. Soc..* **2017**, *139*, 11125-11131.

(17)   Ling, X.; Wang, H.; Huang, S.; Xia, F.; Dresselhaus, M. S. The Renaissance of Black Phosphorus. *Proc. Natl. Acad. Sci. USA* **2015**, *112* (15), 4523.

(18)   Wang, X.; Jones, A. M.; Seyler, K. L.; Tran, V.; Jia, Y.; Zhao, H.; Wang, H.; Yang, L.; Xu, X.; Xia, F. Highly Anisotropic and Robust Excitons in Monolayer Black Phosphorus. *Nat. Nanotechnol.* **2015**, *10*, 517–521.

(19)   Li, L.; Yu, Y.; Ye, G. J.; Ge, Q.; Ou, X.; Wu, H.; Feng, D.; Chen, X. H.; Zhang, Y. Black Phosphorus Field-Effect Transistors. *Nat. Nanotechnol.* **2014**, *9*, 372–377.

(20)   He, J.; He, D.; Wang, Y.; Cui, Q.; Bellus, M. Z.; Chiu, H.-Y.; Zhao, H. Exceptional and Anisotropic Transport Properties of Photocarriers in Black Phosphorus. *ACS Nano* **2015**, *9*, 6436–6442.

(21)   Xiang, D.; Han, C.; Wu, J.; Zhong, S.; Liu, Y.; Lin, J.; Zhang, X.-A.; Ping Hu, W.; Özyilmaz, B.; Neto, A. H. C.; Wee, A. T. S.; Chen, W. Surface Transfer Doping Induced Effective Modulation on Ambipolar Characteristics of Few-Layer Black Phosphorus. *Nat. Commun.* **2015**, *6*, 6485.

(22)   Ryder, C. R.; Wood, J. D.; Wells, S. A.; Yang, Y.; Jariwala, D.; Marks, T. J.; Schatz, G. C.; Hersam, M. C. Covalent Functionalization and Passivation of Exfoliated Black Phosphorus via Aryl Diazonium Chemistry. *Nat. Chem.* **2016**, *8*, 597–602.

(23)   Zhang, L.; Huang, H.; Zhang, B.; Gu, M.; Zhao, D.; Zhao, X.; Li, L.; Zhou, J.; Wu, K.; Cheng, Y.; Zhang, J. Structure and Properties of Violet Phosphorus and Its Phosphorene Exfoliation. *Angew. Chem. Int. Ed.* **2020**, *59*, 1074–1080.

(24)   Schusteritsch, G.; Uhrin, M.; Pickard, C. J. Single-Layered Hittorf's Phosphorus: A Wide-Bandgap High Mobility 2D Material. *Nano Lett.* **2016**, *16*, 2975–2980.

(25)   Lin, S.; Lai, W. K.; Li, Y.; Lu, W.; Bai, G.; Lau, S. P. Liquid-Phase Exfoliation of Violet Phosphorus for Electronic Applications. *SmartMat* **2021**, *2*, 226–233.

(26)   Lin, Z.; Liu, Y.; Halim, U.; Ding, M.; Liu, Y.; Wang, Y.; Jia, C.; Chen, P.; Duan, X.; Wang, C.; Song, F.; Li, M.; Wan, C.; Huang, Y.; Duan, X. Solution-Processable 2D Semiconductors for High-Performance Large-Area Electronics. *Nature* **2018**, *562*, 254–258.

(27)   Zhang, L.; Gu, M.; Li, L.; Zhao, X.; Fu, C.; Liu, T.; Xu, X.; Cheng, Y.; Zhang, J. High Yield Synthesis of Violet Phosphorus Crystals. *Chem. Mater.* **2020**, *32*, 7363–7369.

(28)   Zhang, Z.; Xing, D.-H.; Li, J.; Yan, Q. Hittorf's Phosphorus: The Missing Link during Transformation of Red Phosphorus to Black Phosphorus. *CrystEngComm* **2017**, *19*, 905–909.

(29)   Thurn, H.; Krebs, H. Über Struktur Und Eigenschaften Der Halbmetalle. XXII. Die Kristallstruktur Des Hittorfschen Phosphors. *Acta Crystallogr. B* **1969**, *25*, 125–135.

(30)   Brent, J. R.; Savjani, N.; Lewis, E. A.; Haigh, S. J.; Lewis, D. J.; O'Brien, P. Production of Few-Layer Phosphorene by Liquid Exfoliation of Black Phosphorus. *Chem. Commun.* **2014**, *50*, 13338–13341.

(31) Yasaei, P.; Kumar, B.; Foroozan, T.; Wang, C.; Asadi, M.; Tuschel, D.; Indacochea, J. E.; Klie, R. F.; Salehi-Khojin, A. High-Quality Black Phosphorus Atomic Layers by Liquid-Phase Exfoliation. *Adv. Mater.* **2015**, *27*, 1887–1892.

(32) Fasol, G.; Cardona, M.; Hönle, W.; von Schnering, H. G. Lattice Dynamics of Hittorf's Phosphorus and Identification of Structural Groups and Defects in Amorphous Red Phosphorus. *Solid State Commun.* **1984**, *52*, 307–310.

(33) Zhang, L.; Huang, H.; Lv, Z.; Li, L.; Gu, M.; Zhao, X.; Zhang, B.; Cheng, Y.; Zhang, J. Phonon Properties of Bulk Violet Phosphorus Single Crystals: Temperature and Pressure Evolution. *ACS Appl. Electron. Mater.* **2021**, *3*, 1043–1049.

(34) Wood, J. D.; Wells, S. A.; Jariwala, D.; Chen, K.-S.; Cho, E.; Sangwan, V. K.; Liu, X.; Lauhon, L. J.; Marks, T. J.; Hersam, M. C. Effective Passivation of Exfoliated Black Phosphorus Transistors against Ambient Degradation. *Nano Lett.* **2014**, *14*, 6964–6970.

(35) Yang, S.; Zhang, K.; Ricciardulli, A. G.; Zhang, P.; Liao, Z.; Lohe, M. R.; Zschech, E.; Blom, P. W. M.; Pisula, W.; Müllen, K.; Feng, X. A Delamination Strategy for Thinly Layered Defect-Free High-Mobility Black Phosphorus Flakes. *Angew. Chem. Int. Ed.* **2018**, *57*, 4677–4681.

(36) Mak, K. F.; Lee, C.; Hone, J.; Shan, J.; Heinz, T. F. Atomically Thin MoS2: A New Direct-Gap Semiconductor. *Phys. Rev. Lett.* **2010**, *105*, 136805.

(37) Kotadiya, N. B.; Lu, H.; Mondal, A.; Ie, Y.; Andrienko, D.; Blom, P. W. M.; Wetzelaer, G.-J. A. H. Universal Strategy for Ohmic Hole Injection into Organic Semiconductors with High Ionization Energies. *Nat. Mater.* **2018**, *17*, 329–334.

(38) Wang, Y.; Slassi, A.; Cornil, J.; Beljonne, D.; Samorì, P. Tuning the Optical and Electrical Properties of Few-Layer Black Phosphorus via Physisorption of Small Solvent Molecules. *Small* **2019**, *15*, 1903432.

(39) Kelly, A. G.; Hallam, T.; Backes, C.; Harvey, A.; Esmaeily, A. S.; Godwin, I.; Coelho, J.; Nicolosi, V.; Lauth, J.; Kulkarni, A.; Kinge, S.; Siebbeles, L. D. A.; Duesberg, G. S.; Coleman, J. N. All-Printed Thin-Film Transistors from Networks of Liquid-Exfoliated Nanosheets. *Science* **2017**, *356*, 69–73.

(40) Curreli, N.; Serri, M.; Spirito, D.; Lago, E.; Petroni, E.; Martín-García, B.; Politano, A.; Gürbulak, B.; Duman, S.; Krahne, R.; Pellegrini, V.; Bonaccorso, F. Liquid Phase Exfoliated Indium Selenide Based Highly Sensitive Photodetectors. *Adv. Funct. Mater.* **2020**, *30*, 1908427.

(41) Ippolito, S.; Kelly, A. G.; Furlan de Oliveira, R.; Stoeckel, M.-A.; Iglesias, D.; Roy, A.; Downing, C.; Bian, Z.; Lombardi, L.; Samad, Y. A.; Nicolosi, V.; Ferrari, A. C.; Coleman, J. N.; Samorì, P. Covalently Interconnected Transition Metal Dichalcogenide Networks via Defect Engineering for High-Performance Electronic Devices. *Nat. Nanotechnol.* **2021**, *16*, 592–598.

(42) Kelly, A. G.; O'Suilleabhain, D.; Gabbett, C.; Coleman, J. N. The Electrical Conductivity of Solution-Processed Nanosheet Networks. *Nat. Rev. Mater.* **2021**, 1–18.

(43) Hu, P.; Wen, Z.; Wang, L.; Tan, P.; Xiao, K. Synthesis of Few-Layer GaSe Nanosheets for High Performance Photodetectors. *ACS Nano* **2012**, *6*, 5988–5994.

(44) Lau, C. S.; Chee, J. Y.; Ang, Y. S.; Tong, S. W.; Cao, L.; Ooi, Z.-E.; Wang, T.; Ang, L. K.; Wang, Y.; Chhowalla, M.; Goh, K. E. J. Quantum Transport in Two-Dimensional WS2 with High-Efficiency Carrier Injection through Indium Alloy Contacts. *ACS Nano* **2020**, *14*, 13700–13708.

(45) Fali, A.; Snure, M..; Abate, Y. Violet phosphorus surface chemical degradation in comparison to black phosphorus. *Appl. Phys. Lett.* **2021**, *118*, 163105.